Comparative analysis of polarimetric SAR images based on multi-target decomposition

M A Elenean[1], A K Helmy[2], F Eltohamy[1], A Azouz[1]

[1] Electrical Engineering Department, Military Technical College, Cairo, Egypt
[2] National Authority of Remote Sensing and Space Sciences, 23 Joseph Tito St, Cairo, Egypt

E-mail: m.aboelenean@ieee.org

Abstract.

A novel approach for PolSAR image analysis using support vector machines (SVM) were presented in this paper, with a focus on the impact of target decomposition techniques on classification accuracy. We explore the use of six different target decomposition techniques, including Cloude, Huynen, HAAlpha, Freeman, Vanzyl, and Yamaguchi, to extract feature vectors for training SVM models. Our study evaluates the performance of the classifiers on two standard benchmark datasets (Flevoland and San Francisco Bay) using multiple assessment metrics, including accuracy, sensitivity/recall, specificity, precision, F1-score, and Kappa coefficient. Our contribution is twofold: first, we provide a comprehensive analysis of how the choice of target decomposition technique affects the classification accuracy of PolSAR images using SVMs, and second, we demonstrate the effectiveness of SVMs for PolSAR image classification, particularly for differentiating between different land cover types. Our results show that certain target decomposition techniques are better suited for specific land cover types, and our approach can achieve high classification accuracy across different datasets. Overall, our study provides important insights into the effective use of SVMs and target decomposition techniques for PolSAR image analysis.

Keywords: SVM, PolSAR images, land cover classification, target decomposition techniques, Cloude, Huynen, HAAlpha, Freeman, Vanzyl, Yamaguch.

1. Introduction

Polarimetric Synthetic Aperture Radar (PolSAR) is a sophisticated form of Synthetic Aperture Radar (SAR). It involves the emission and reception of radar waves in various polarization modes. It provides more information about the target scene compared to traditional single polarization SAR. PolSAR images have numerous applications in remote sensing, including land use and cover classification, change monitoring, disaster risk assessment, and urban analysis. In recent years, there has been an abundance of PolSAR data provided by various airborne and space-borne SAR systems such as AIRSAR, UAVSAR, SENTINEL-1, TSX, RADARSAT-2 and ALOS-PolSAR. However, manual analysis of this large volume of complex images is not feasible, hence the need for the development of autonomous or semi-automatic systems or models for PolSAR image analysis and information extraction has become imperative [1], [2], [3].

This paper focuses on the use of supervised classification methods, particularly Support Vector Machines (SVMs), for the analysis of (PolSAR) images. Various target decomposition techniques such as (Cloude, Huynen, HAAlpha, Freeman, Vanzyl, and Yamaguchi) are used

to extract feature vectors from fully polarimetric data, which are then used to train the SVM model. The choice of target decomposition technique has a major effect on the overall classification accuracy. The effectiveness of various target decomposition techniques is evaluated using two benchmark datasets: the AirSAR mission over the Flevoland area and the Radarsat-2 satellite mission over San Francisco Bay [4]. The used evaluation parameters include accuracy, sensitivity/recall, specificity, precision, F1-score, and Kappa coefficient [5], [6], [7]. The key contribution of this paper is to enhance the understanding of PolSAR image classification using supervised methods and the impact of various target decomposition techniques in classification accuracy. The results of this study provide valuable insights for practitioners and researchers in the field of microwave remote sensing.

The paper is organized into four sections. It includes an introduction, target decomposition theorems, a description of the SVM algorithm, and an implementation of the SVM-based land cover classification model and performance evaluation, and the conclusion.

2. Target Decomposition Theorems

The polarization diversity in PolSAR makes it a valuable tool for terrain surface classification. Many widely used classification methods are based on polarimetric decomposition. The received radar signal is encoded in a scattering matrix **S**, defined as:

$$\mathbf{S} = \begin{bmatrix} S_{hh} & S_{hv} \\ S_{vh} & S_{vv} \end{bmatrix} \tag{1}$$

where for monostatic cases, the matrix **S** is symmetrical, $S_{hv} = S_{vh}$. For complex targets, the scattering matrix is not adequate. A possible alternative is the representation based on second-order polarimetry, such as the coherency matrix T_3 and the covariance matrix C_3. The scattering matrix **S** can be transformed into a vector k_p using Pauli basis:

$$k_p = \frac{1}{\sqrt{2}} \left[S_{hh} + S_{vv}, S_{hh} - S_{vv}, 2S_{hv} \right]^T \tag{2}$$

Then, the (3×3) coherency matrix T_3 can be defined as:

$$T_3 = k_p . k_p^{*T} \tag{3}$$

Where * denotes complex conjugation.

Target decomposition theorems aim to provide an interpretation of scattering interactions by accounting for physical constraints such as the invariance of the average target to changes in wave polarization basis. The first formalization of these theorems was by Huynen, but their roots can be traced back to Chandrasekhar's work on light scattering by small anisotropic particles. Then different decomposition methods have been proposed by authors such as Holm and Barnes, Yang, Freeman and Durden, Yamaguchi, Dong, Cloude, vanZyl, Cloude and Pottier [8], [9], [10], [11]. some of this methods are briefly explained in the next subsections.

2.1. Huynen Decomposition

Huynen's decomposition is a method in radar target analysis that separates incoming data into two parts: the single mean target, T_0, and a residual component known as the N-target, T_N. This method uses the Kennaugh matrix or the coherency T_3 matrix to represent the average distributed target in clutter environments. The T_3 matrix is decomposed into T_0 and T_N by incoherent averaging. T_0 represents symmetric target parameters and is dependent on target

tilt angle, while T_N represents nonsymmetric target parameters and remains unchanged with target tilt angle. The N-target is roll invariant, meaning it is independent of rotation along the line of sight. The parameters $(B_{0\ \mathrm{N}}, B_{\mathrm{N}}, E_{\mathrm{N}}, F_{\mathrm{N}})$ are generated from understanding of the mean Kennaugh matrix [9], where the full derivation exist.

2.2. Model-Based Decompositions (Three-Component Decomposition)

In the model-based decomposition approach, the scattering matrix S is separated into various scattering mechanisms in the target medium. The technique was introduced by Freeman and Durden in 1998 [12], and it decomposes the covariance matrix into canopy scatter, even-bounce scatter, and Bragg scatter. This composite scattering model is useful in discriminating different land covers, such as flooded and non-flooded areas, forested and deforested areas, etc.

The first-order Bragg scattering's associated scattering matrix, such as surface scattering and coherent odd-bounce scattering, can be expressed as a 2x2 matrix, where the coefficients that describe the reflection of horizontally and vertically polarized waves are based on the angle of local incidence and the surface's relative dielectric constant. The surface scattering covariance matrix is also expressed as a 3x3 matrix, where the effect of single-bounce scattering is represented by a factor f_S, and the scattering matrix for a dihedral scatterer, which represents even/double-bounce scattering, can be modeled as a 2x2 matrix. The reflection of the backscattered signal from a corner reflector with two sides, such as a building, can be used to mimic double-bounce scattering. The backscatter from a reflective surface made up of various dielectric materials, like a dihedral corner reflector, is analyzed. The reflection coefficients and phase changes are taken into consideration to model the scattering.

The model-based decomposition approach provides a unique solution by making assumptions about the structure of the target surface and provides a more detailed description of the scattering mechanisms compared to other decomposition types.

2.3. EigenVector-Based Decompositions

describes the decomposition of the Hermitian positive semidefinite coherency matrix $\boldsymbol{T}_3$ into three separate targets, each with a single scattering mechanism. This decomposition is achieved through finding the eigenvectors of $\boldsymbol{T}_3$. A target is considered "pure" if it has only one non-zero eigenvalue, while a "random" target lacks any structured polarization and has equal eigenvalues. If the eigenvalues are non-zero and unequal, the target is referred to as partially polarized.

One approach to analyzing the polarimetric behavior of such a target is the Cloude decomposition, which was first proposed by Cloude. This method finds the largest eigenvalue, which represents the dominant scattering mechanism, and creates a target vector with the square root of that eigenvalue and the corresponding eigenvector. The target vector can then be used to calculate the scattering matrix.

The H-Alpha and Cloude decomposition methods using an eigenvector or eigenvalues analysis of the covariance $\boldsymbol{C}_3$ or coherency matrix $\boldsymbol{T}_3$ are briefly explained in the next sections.

2.3.1. Cloude Decomposition: Cloude was the first to suggest an eigenvector-based decomposition, as cited in the publications [13], [14]. He proposed an approach for determining the primary scattering mechanism by locating the biggest eigenvalue (λ_1). The resulting coherency matrix T_1 has a rank of one, has a corresponding scattering matrix S, and can be written as the outer product of a particular target vector $\boldsymbol{k}_1$.

$$\boldsymbol{T}_1 = \lambda_1 \boldsymbol{u}_1 \cdot u_1^{*\ \mathrm{T}} = \boldsymbol{k}_1 \cdot \boldsymbol{k}_1^{*\ \mathrm{T}} \tag{4}$$

Following the Cloude decomposition, the target vector can be represented as follows:

$$\boldsymbol{k}_1 = \sqrt{\lambda_1}\boldsymbol{u}_1 = \frac{\mathrm{e}^{j\phi}}{\sqrt{2A_0}} \begin{bmatrix} 2A_0 \\ C + jD \\ H - jG \end{bmatrix} = \mathrm{e}^{j\phi} \begin{bmatrix} \sqrt{2A_0} \\ \sqrt{B_0 + B}\mathrm{e}^{+j \arctan(D/C)} \\ \sqrt{B_0 - B}\mathrm{e}^{-j \arctan(G/H)} \end{bmatrix} \tag{5}$$

The polarimetric representation of the target vector $\boldsymbol{k_I}$ includes three basic scattering mechanisms, which are surface scattering, dihedral scattering, and volume scattering. These mechanisms can be identified from the three components, or target generators, of the target vector. The characteristics of these mechanisms are as follows:

- For surface scattering, A_0 is much larger than $B_0 + B$ and $B_0 - B$.
- In dihedral scattering, $B_0 + B$ is much larger than A_0 and $B_0 - B$.
- And for volume scattering, $B_0 - B$ is much greater than A_0 and $B_0 + B$.

The application of the target decomposition resulting from Cloude methods is shown in Fig.1. Where the three components of the equivalent unique target $\boldsymbol{T_1}$ are depicted as generators.

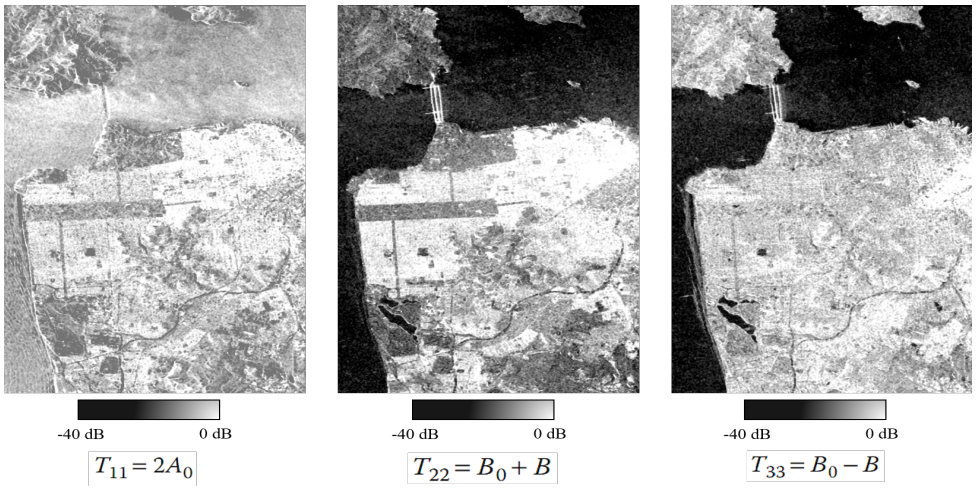

Figure 1: Cloude target decomposition, showcasing the reconstruction of the three generators

2.3.2. H-Alpha Decomposition: The H-Alpha decomposition is a method that leverages the eigen-decomposition of the coherency matrix T_3 [15]. The H-Alpha decomposition is based on three main parameters:

- Alpha Angle (α_i): This is an angle that represents the degree of polarization of the scattering mechanism and can be used to distinguish between different types of scattering. The Alpha angle is given by $\alpha_i = \arccos\left(\frac{\lambda_3}{\sqrt{\lambda_1^2+\lambda_2^2+\lambda_3^2}}\right)$.
- Beta Angle (β_i): This is the angle between the direction of maximum coherence and the horizontal direction. It provides information about the orientation of the scattering mechanism.
- Gamma Angle (γ_i): This is the phase difference between the $(Shh + Svv)$ and S_{hv} terms, and provides information about the ellipticity of the scattering mechanism.

The Alpha angle can be used to distinguish between volume scattering and surface scattering Fig. 2, while the Beta angle provides information about the orientation of the scattering mechanism. The Gamma angle provides information about the ellipticity of the scattering

mechanism. These parameters are used to distinguish between different scattering mechanisms and to extract additional information about the target's properties, For example:

- The polarimetric scattering entropy H is defined by:

$$H = \sum_i P_i log_3 P_i \tag{6}$$

Where

$$P_i = \frac{\lambda_i}{\sum_i \lambda_i} \tag{7}$$

- Average alpha α angle defined by:

$$\bar{\alpha} = \sum_i \alpha_i P_i \tag{8}$$

- Anisotropy A described as:

$$A = \frac{\lambda_2 - \lambda_3}{\lambda_2 + \lambda_3} \tag{9}$$

The normalization of eigenvalues is represented by P_i, while H represents entropy that gauges the randomness of the scattering medium.

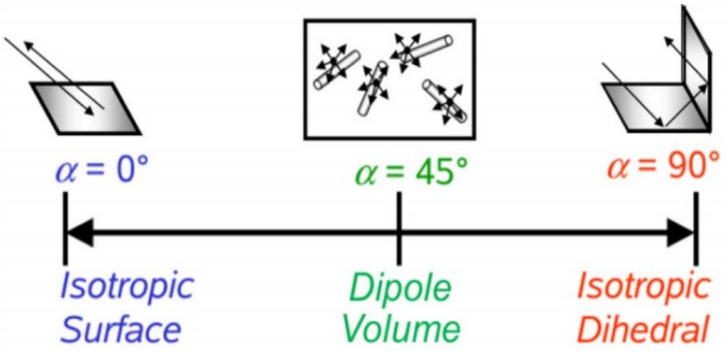

Figure 2: Alpha Ranges Vs. Scattering Mechanisms.

From this analysis two main features (H , $\bar{\alpha}$) are enough to separate different types of scattering behavior into nine zones corresponds to nine different scattering mechanisms as shown in Fig. 3.

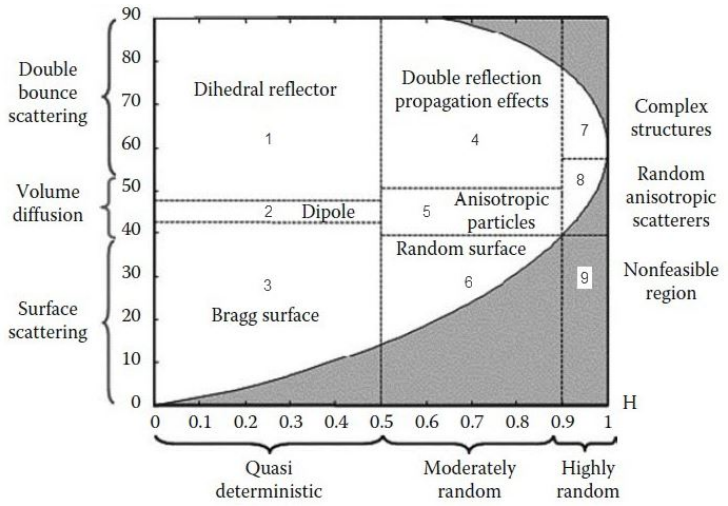

Figure 3: (H − $\bar{\alpha}$) decomposition plane.

From the previous target decompositions analysis. In this paper we used a combination of six different target decompositions such as (Huynen, Cloude, H-A Alpha, Freeman and Durden, Yamaguchi and Van-Zyl) to extract the polarimetric feature components from the fully polarimetric SAR data. Each of which has a specific criterion in identifying the scattering process. These features are then used to traine out the SVM model, which will be discussed in the next section.

3. Support Vector Machines (SVM)

SVM is a type of supervised learning method used for classification, regression and outlier detection. It aims to map high-dimensional data to a lower dimensional space by finding a linear hyperplane that maximizes the margin between classes. This is achieved through the use of a kernel function that maps the data to a higher dimensional feature space where the hyperplane is optimized. The optimization is performed by finding the hyperplane that has maximum distance to all training examples from different classes in the feature space [16–20]. Support Vector Machines (SVMs) have several benefits that have contributed to their popularity. Firstly, they are able to perform well even in situations where the number of dimensions is large. Secondly, they can be adapted to a variety of situations through the use of different kernel functions. Additionally, SVMs are designed to use memory efficiently. Despite these advantages, it is important to note that if the number of features is significantly higher than the number of samples, there is a risk of overfitting. Furthermore, SVMs do not output probability estimates directly. SVMs can be applied to a range of machine learning tasks, including linear classification, non-linear classification, and regression.

The optimal hyperplanes separation in SVM is performed by finding a decision function, which is a function of $\vec{x}$, that separates two classes of data. By finding the function that satisfies the condition $y_i \cdot \text{sgn}(f(\vec{x})) > 0$ the objective of the binary classifier is satisfied. For linear separable case, the decision function is defined as $f(\vec{x}) = \langle \vec{w} \cdot \vec{x} \rangle + b$. The optimal hyperplanes separation is obtained by maximizing the margin between the two classes and the rest of the data satisfies the constraint $y_i \cdot \text{sgn}(\langle \vec{w} \cdot \vec{x}_i \rangle + b) \geq 1$.

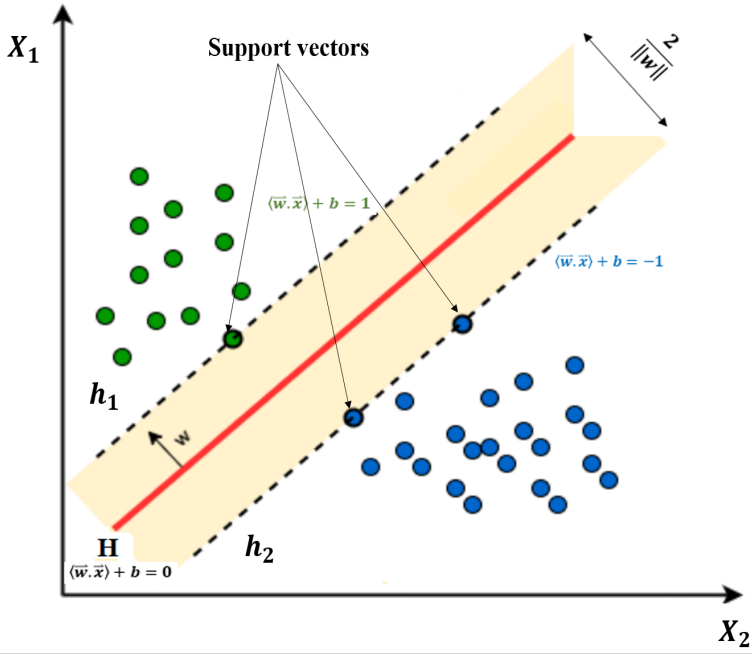

Figure 4: Concept of optimal separating hyperplanes between two classes

An illustration of geometry in two-dimensional feature space is shown in Fig.4. The separating hyperplane is H, followed by h_1 and h_2, while the green and blue class points denote two different sorts of samples. Support vectors are the sample data on h_1 and h_2, which satisfy $\langle \vec{w} \cdot \vec{x} \rangle + b = 1$ or $\langle \vec{w} \cdot \vec{x} \rangle + b = -1$. The distance between the separating hyperplane is called margin.

In PolSAR data classification, the samples are usually divided into more than two categories, which requires a multi-classifier. There are two common methods for multi-classification: one-vs-all and one-vs-one [16–19].

The one-vs-all method consists of using a binary classifier for each category, with the samples of category i treated as positive samples and the samples of all other categories treated as negative samples. In total, N binary classifiers are required for an N-category problem. This method is often preferred due to its reduced runtime while still providing similar results to the other method. The one-vs-one method, on the other hand, requires $k = N(N-1)/2$ binary classifiers, where each classifier compares two categories and the final category is determined by a vote among the classifiers. This method provides a more comprehensive comparison of the categories but requires a larger computational effort.

4. SVM-based Classification model Implementaion and Experimental results

The PolSAR image is a well-known scattering map that represents the distinct scattering properties of various objects and targets based on different polarization combinations. To classify the land cover of PolSAR images, a robust and efficient Support Vector Machine (SVM) model is developed by utilizing the physical and structural properties of PolSAR data. The features are extracted from the scattering mechanisms derived from multi-target decompositions, which are then used to train the SVM models to perform the classification task.

The Flowchart of the SVM-based land cover classification model for PolSAR data is illustrated in Fig.5. As shown the process of using SVM for land cover classification of PolSAR images can be broken down into five key steps:

(1) Preprocessing: The first step involves extracting the scattering matrix and calculating the coherency matrix T3, as well as cleaning the images through the application of filters to remove speckle noise and improve image quality.

(2) Feature extraction: The images are then analyzed to extract relevant features that will be used as input for the SVM classifier. These features include intensity, entropy, coherence, and texture and are related to polarimetric target decomposition techniques which divide the target into different components based on their scattering characteristics.

(3) Model training: The extracted features are then used to train the SVM classifier with a set of training data. The model is optimized for performance on test data.

(4) Model validation: To ensure accuracy, the model is tested with a set of validation data that is separate from the training set.

(5) Classification: Finally, the model is used for the actual classification process.

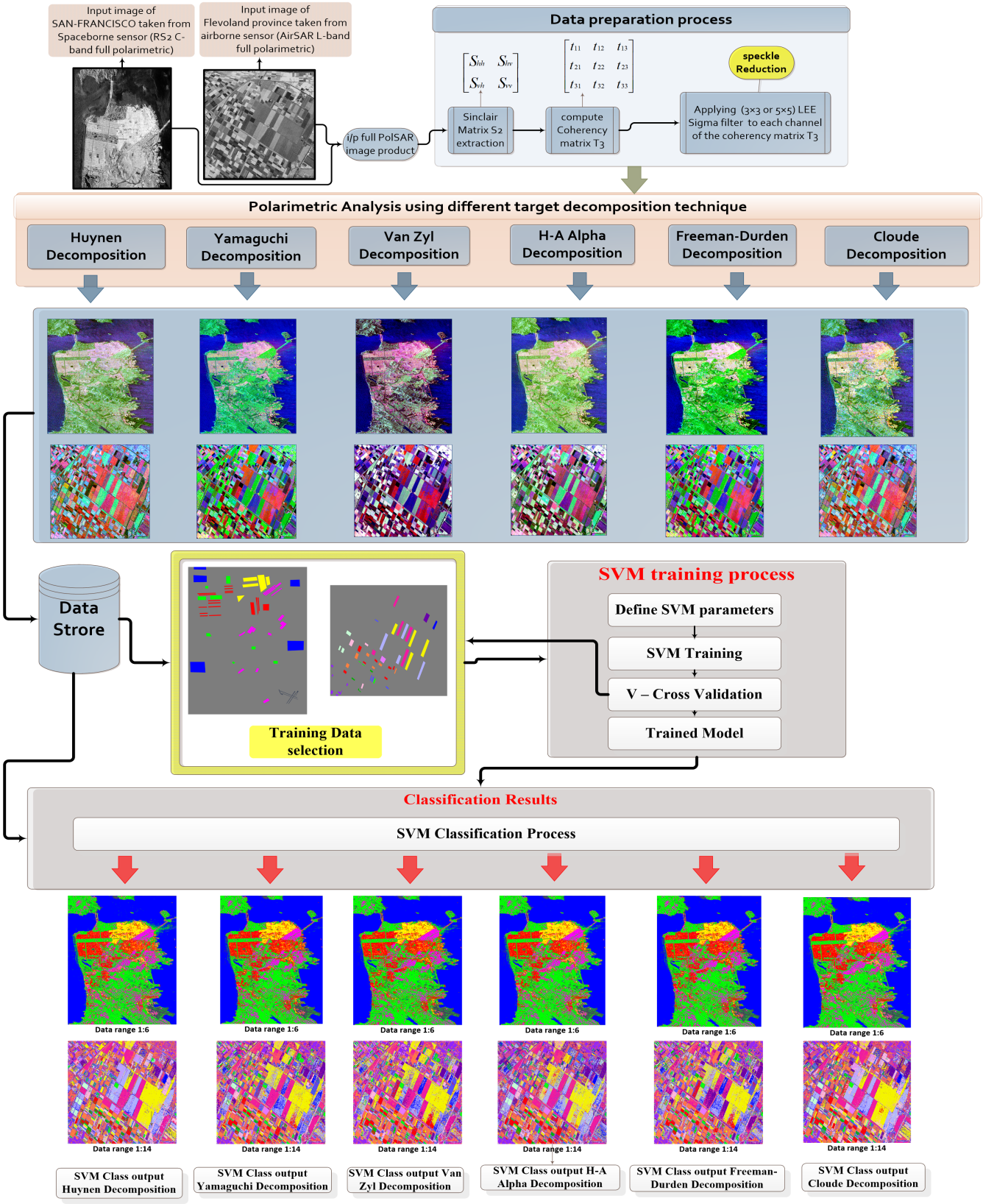

Figure 5: Flowchart of the proposed SVM-based land cover classification model for PolSAR data

4.1. Experimental results and the Performance Evaluation

Two real PolSAR datasets, the Flevoland province and San Francisco Bay, Fig.6, are used for comparative study purposes. The Flevoland dataset is aimed at crop classification while the San Francisco Bay dataset focuses on land cover classification. This allows for testing the classification model on different applications and evaluating its robustness. These datasets are widely used in PolSAR image analysis studies [4], and their corresponding ground truth maps provide a solid foundation for quantitative assessment. The data was collected by NASA/JPL's AirSAR aircraft mission and Radar-Sat2 (RS2) satellite mission, respectively. The AirSAR dataset was obtained in L-band and the RS2 dataset in C-band, both utilizing full polarimetric imaging channels. Technical Specifications of the Datasets Used is illustrated in Table 1. The use of different sources, AirSAR and RS2, with varying spatial and radiometric resolutions, increases the likelihood that the results will be generalized to other Datasets.

Table 1: Technical specifications of datasets

Dataset	Source	Band	Polarization	Ground Resolution	Classes	Area	Acquisition Year
Flevoland Province	AirSAR	L-band	4-channels	6.7 m (Range), 12.2 m (Azimuth)	14	1020 x 1024 pixels	1991
San Francisco Bay	RADARSAT-2	C-band	4-channels	4.7 m (Range), 4.8 m (Azimuth)	6	3074 x 1944 pixels	2008

The Pauli-RGB color composite image of the Flevoland province and its ground-truth map are depicted in Fig. 6 (a, b). As per the legend, the image displays various agricultural zones with crops of diverse species, resulting in 14 different classes. Fig. 6 (c, d) shows the Pauli-RGB color composite image of the San Francisco Bay area along with the accompanying optical image obtained from Google Earth. This Dataset consists of key land cover types, including urban areas with three different patterns and structures, water bodies, and forest or open regions. Urban areas correspond to an even or double-bounce scattering, water bodies and asphalt (runways-aprons) correspond to Bragg surface scattering, and forest or open areas correspond to canopy or volume scattering.

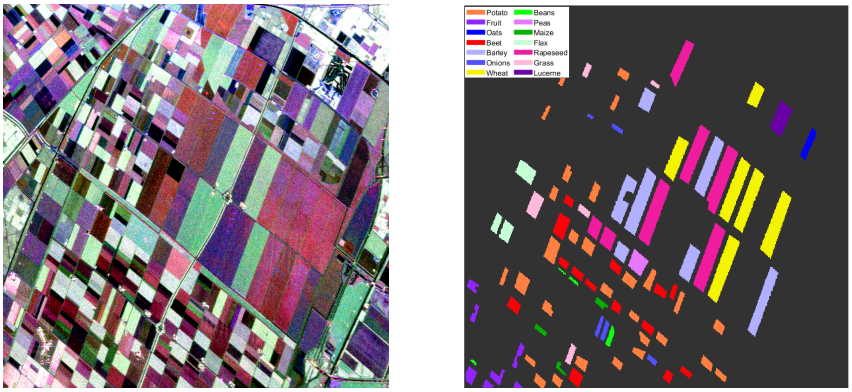

(a) (b)

Figure 6: The dataset used for analysis. (a) Flevoland Pauli-RGB image; (b) FL related ground truth map; (c) San Francisco Pauli-RGB image; (d) SF optical image

(c) (d)

Figure 6. Continue.

The SVM-based classification model is applied to the Flevoland and San Francisco Bay datasets as per the flowchart in Fig.5. The pre-processing phase, including the calculation of the coherency matrix and the reduction of speckle noise using the Lee sigma filter, precedes the selection of polarimetric features. The aim of this process is to evaluate the robustness and accuracy of the SVM classifier in separating different classes.

For the AirSAR (Flevoland) dataset, the training and test data are selected in such a way as to cover all 14 crop species present in the image, using the available ground truth information. For the RADARSAT-2 (San Francisco) dataset, the selection focuses on the six main land cover types recognized from the optical image obtained from Google Earth.

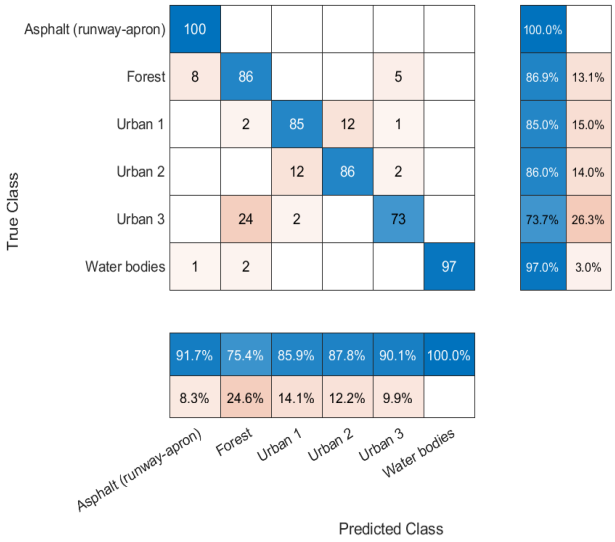

(a)

Figure 7: Example of confusion matrix. (a) CM computed over San Francisco dataset; (b) CM computed over Flevoland dataset

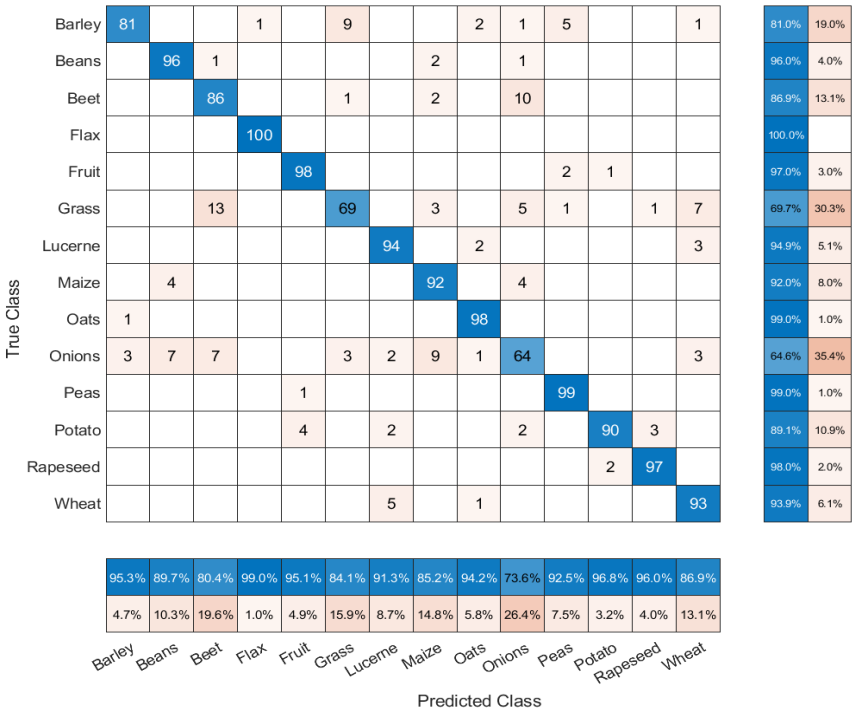

(b)

Figure 7. Continue.

The trained SVM classifier is then used to perform the label prediction task. The results of the classification model are evaluated using cross-validation with the ground truth samples (*Chi et al., 2008*). The confusion matrix, as shown in Fig.7, is used to assess the performance of the classification model on test data where the true values are known. The evaluation metrics: accuracy, sensitivity/recall, specificity, precision, F1-score, and Kappa coefficient, are calculated from the confusion matrix to understand the performance and behavior of the classification model under different decomposition types. A column summary, which is normalized by column, presents the accuracy and in accuracy of categorization for each predicted class as a percentage of the total number of observations for that particular class. A row summary, normalized by row, displays the ratio of correctly and incorrectly categorized observations for each true class out of the total number of observations for that class.

In order to visually evaluate the classification results produced by the SVM-based model for different target decompositions. These results are visualized by overlaying the ground truth information for both the Flevoland province and San Francisco Bay datasets. Figures (8, 9) provides a clear representation of the performance of the SVM-based classification model for different target decompositions.

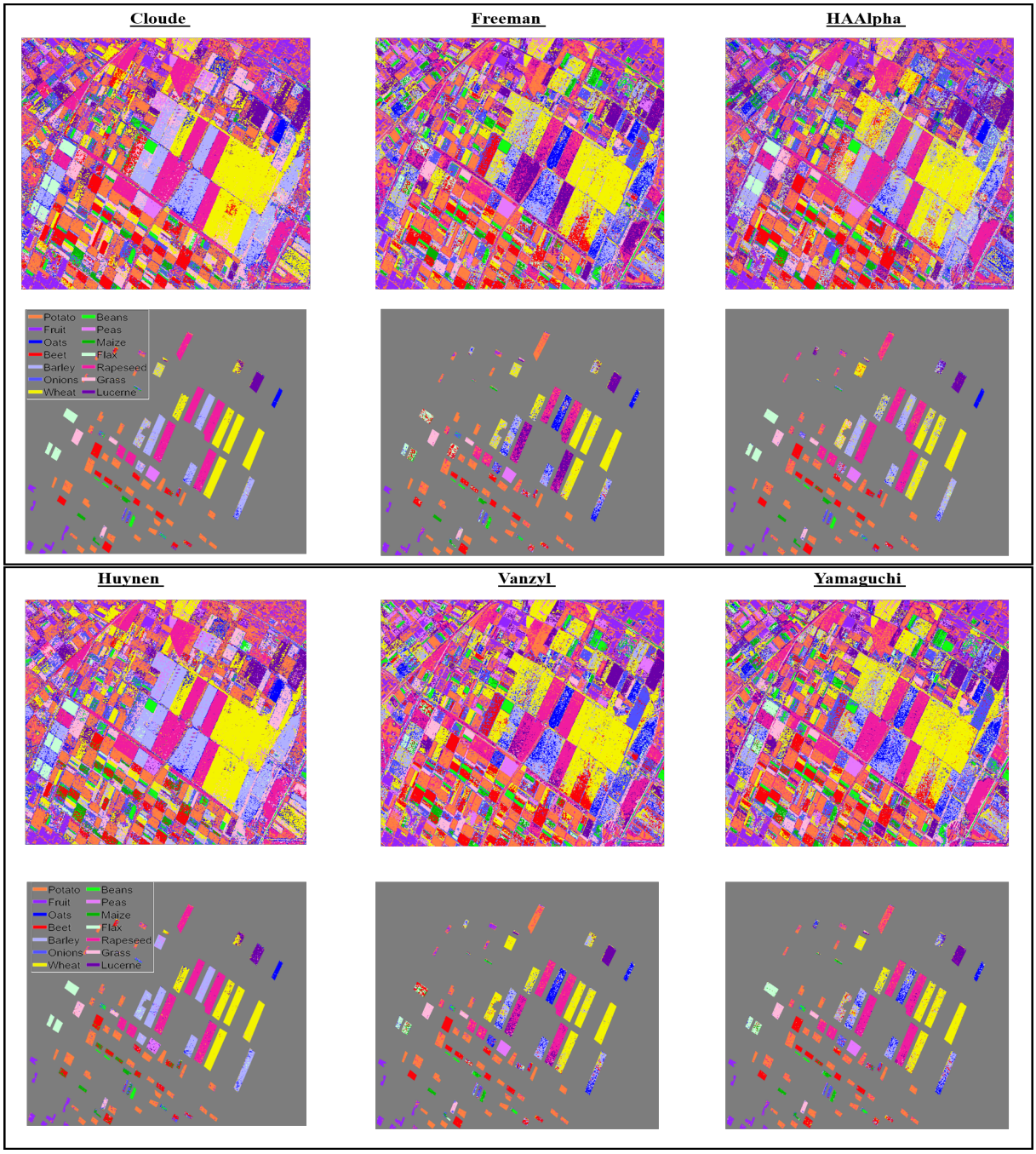

Figure 8: Classification model output over Flevoland dataset

As shown in Fig.8, a comparative analysis of the classification results of the SVM-based model is performed at different target decompositions using the Flevoland dataset. The first and third rows of the figure depict the model outputs obtained at each target decomposition, with the (Cloude - Freeman and durden - HAAlpha) decompositions shown in the first row and (Huynen - VanZyl - Yamaguchi) shown in the third row. The second and fourth rows, on the other hand, present a comparison of the classification results overlaid the ground truth information.

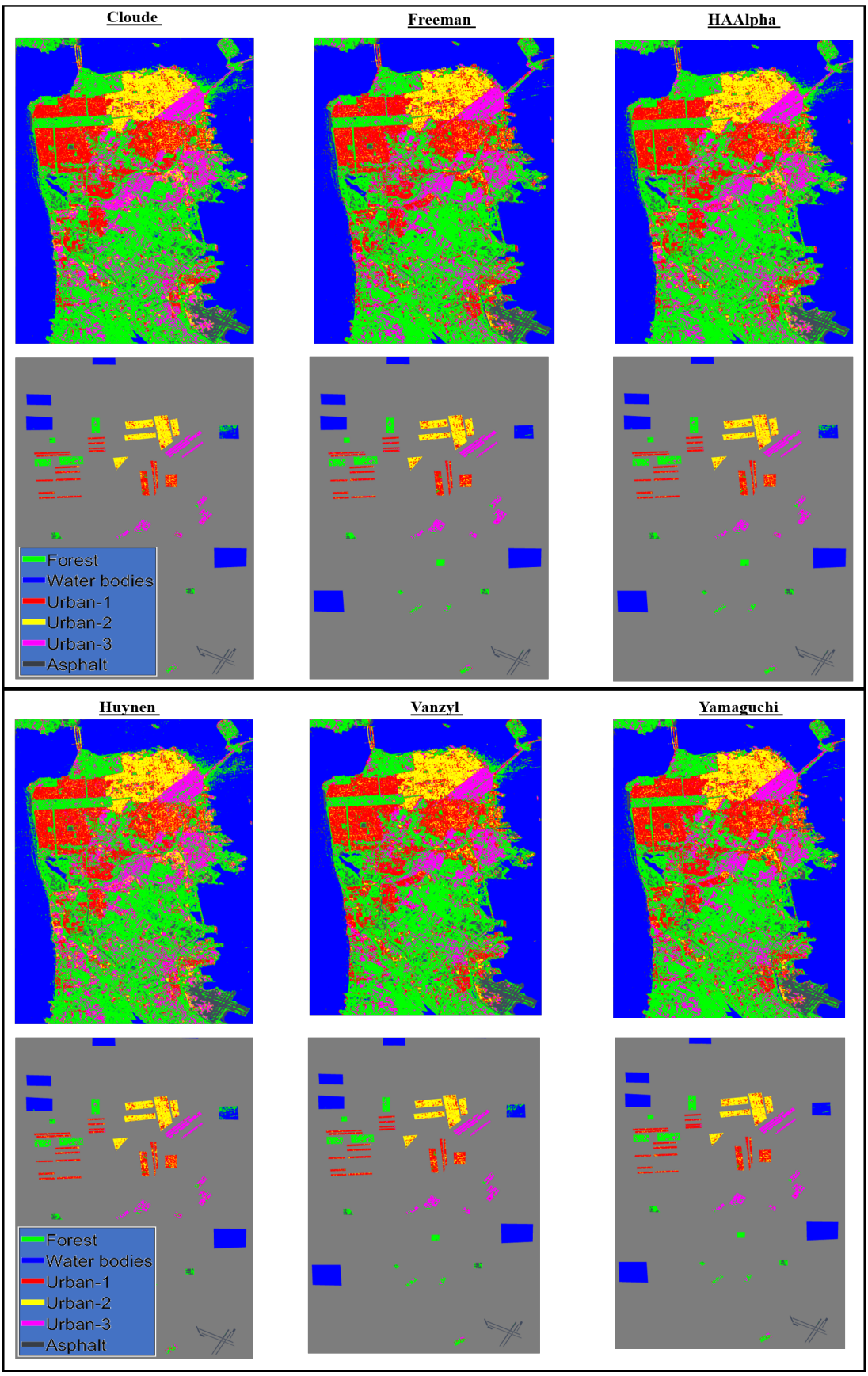

Figure 9: Classification model output over San-Francisco dataset

Also a comparative analysis of the classification results of the SVM-based model is performed at different target decompositions using the San_Francisco dataset are shown in Fig.9.

This comparative analysis provides insights into the performance and accuracy of the SVM-based model at different target decompositions. The evaluation of the relationship between accuracy and target decomposition revealed that different decomposition techniques exhibit varying ability in identifying specific class types.

Table 2: Evaluation parameters of SVM_based classifier at each target decomposition type

SVMs Evaluation parameters of Flevoland Dataset							
Decomposition type	**Original T3**	**Cloude**	**Huynen**	**HAAlpha**	**Freeman**	**Vanzyl**	**Yamaguchi**
Accuracy	84.18%	90.10%	89.37%	80.09%	69.55%	72.78%	78.59%
Sensitivity/Recall	83.00%	89.75%	86.18%	86.56%	75.56%	72.23%	78.43%
Specificity	98.77%	99.25%	99.20%	98.37%	97.61%	97.84%	98.29%
Precision	70.76%	77.45%	73.44%	74.24%	65.62%	63.54%	69.61%
F1_score	74.54%	82.17%	77.54%	78.77%	66.15%	64.54%	71.33%
Kappa Coefficient	81.57%	88.44%	87.56%	76.76%	65.13%	68.50%	75.10%
SVMs Evaluation parameters of San Francisco Dataset							
Decomposition type	**Original T3**	**Cloude**	**Huynen**	**HAAlpha**	**Freeman**	**Vanzyl**	**Yamaguchi**
Accuracy	89.34%	89.83%	87.24%	89.48%	90.07%	89.53%	90.17%
Sensitivity/Recall	86.91%	87.99%	84.97%	87.55%	87.80%	87.43%	87.89%
Specificity	97.99%	98.09%	97.58%	98.02%	98.12%	98.03%	98.14%
Precision	81.31%	81.96%	78.84%	81.57%	82.50%	81.43%	82.71%
F1_score	83.21%	83.82%	80.71%	83.38%	84.27%	83.29%	84.42%
Kappa Coefficient	85.20%	85.94%	82.37%	85.45%	86.21%	85.51%	86.34%

The results in Table 2 provide a comparison of the performance of SVM classifier on two datasets, after applying various target decomposition techniques. The same evaluation parameters are used to assess the performance of the classifiers.

For the Flevoland dataset, the highest accuracy was 90.10% obtained using the Cloude decomposition type, the highest sensitivity/recall was 89.75% obtained using the Cloude decomposition type as well. Also the highest specificity was 99.25%, the highest precision was 77.45% , the highest F1 score was 82.17%, and the highest Kappa coefficient was 88.44% all obtained using the Cloude decomposition which is an Eigenvalues and Eigenvectors based decomposition type.

For the San Francisco dataset, the highest accuracy was 90.17% obtained using the Yamaguchi decomposition type, the highest sensitivity/recall was 87.89% obtained using the Yamaguchi decomposition type as well. Also the highest specificity was 98.14%, the highest precision was 82.71% , the highest F1 score was 84.42%, and the highest Kappa coefficient was 86.34% all obtained using the Yamaguchi decomposition which is model-based decomposition type.

These results indicates that the Cloude decomposition technique, which is based on eigenvalue and eigenvector analysis, is the best option for analyzing crop types in the Flevoland dataset. Conversely, the Yamaguchi decomposition technique, a model-based approach, performed better when analyzing landcover in the San Francisco dataset. It is important to note that each decomposition technique has its own underlying basis and the choice of which to use will depend on the specific analysis being performed.

Fig.10, shows a bar-chart of the overall statistical results of the SVM-based classification model, for all target decomposition methods utilized in terms of accuracy and kappa coefficient.

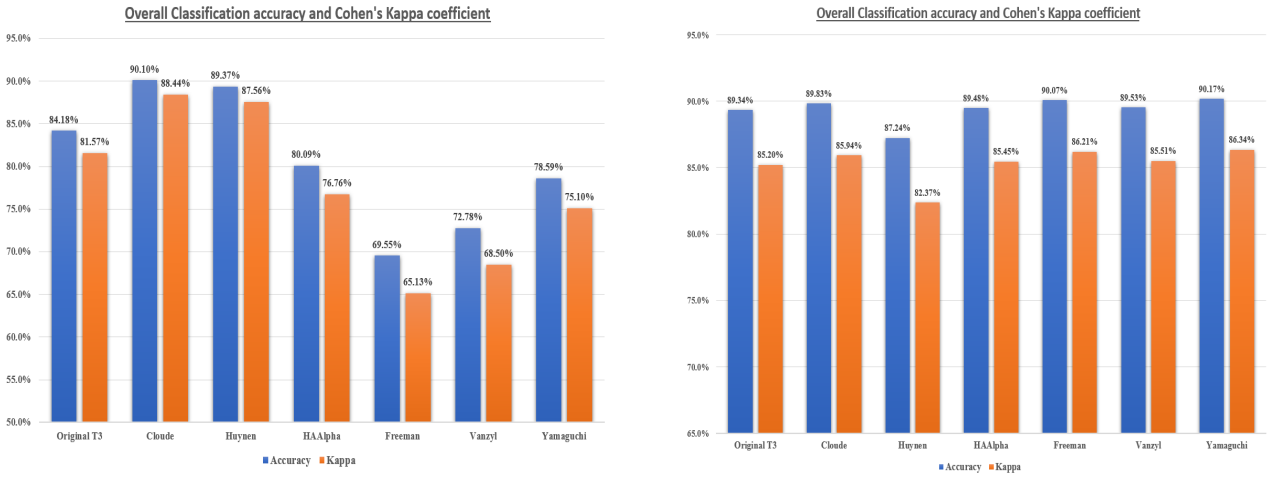

(a) Statistical results on Flevoland dataset

(b) Statistical results on San Francisco dataset

Figure 10: bar-chart of the overall statistical results in terms of accuracy and kappa coefficient.

From the figure, it appears that Cloude decomposition is well suited for the Flevoland dataset due to its eigenvalue and eigenvector analysis, while the model-based approach of the Yamaguchi decomposition made it the better choice for the landcover analysis in the San Francisco dataset.

5. Conclusion

In this paper, the implementation of a SVM-based classification model for PolSAR data was developed. The model is designed to analyze the performance of different decomposition techniques in the classification process. Two frequently used datasets are employed for the comparative analysis, the AirSAR dataset over the Flevoland area and the Radarsat-2 dataset over the San Francisco Bay. The results showed that the Cloude decomposition technique, which is based on eigen value and eigen vector analysis, was more effective for crop type analysis using the Flevoland dataset. On the other hand, the Yamaguchi decomposition technique, which is model-based, performed better for landcover analysis using the San Francisco dataset. These findings highlight the importance of considering the specific characteristics of both the dataset and the analysis goals when choosing the appropriate decomposition technique.

References

[1] Fouad M, Elbohy A, Mashaly A, Abosekeen A, Abdalla A and Azouz A 2022 *The Egy. Journal of RS and Space Science* **25** 659–671
[2] Yu L, Zeng Z, Liu A, Xie X, Wang H, Xu F and Hong W 2022 *IEEE J. of Selected Topics in Applied EORS* **15** 930–943
[3] Elenean M A, Hafez A, Helmy A, ElTohamy F and Azouz A 2023 Unsupervised multi-level segmentation framework for polsar data using h-alpha features and the combined edge-region based segmentation *2023 IEEE Aerospace Conference* (IEEE) pp 1–8
[4] Liu X, Jiao L, Tang X, Sun Q and Zhang D 2018 *IEEE Transactions on Geoscience and RS* **57** 3040–3054
[5] Tien Bui D, Shahabi H, Shirzadi A, Chapi K, Alizadeh M, Chen W, Mohammadi A, Ahmad B B, Panahi M, Hong H *et al* 2018 *Remote Sensing* **10** 1527
[6] Jing H, Wang Z, Sun X, Xiao D and Fu K 2021 *IEEE J. of Selected Topics in Applied EO and RS* **14** 10716–10732
[7] Hou B, Guan J, Wu Q and Jiao L 2019 *IEEE Geoscience and Remote Sensing Letters* **17** 1737–1741
[8] Ferguson J E and Gunn G E 2022 *RS of Environment* **280** 113176
[9] Lee J S and Pottier E 2017 *Polarimetric radar imaging: from basics to applications* (CRC press)
[10] Souyris J C, Henry C and Adragna F 2003 *IEEE Transactions on Geoscience and RS* **41** 2725–2734

[11] Cloude S R and Pottier E 1996 *IEEE transactions on geoscience and RS* **34** 498–518
[12] Freeman A and Durden S L 1998 *IEEE transactions on geoscience and RS* **36** 963–973
[13] Schuler D L, Lee J S and Kasilingam D 2006 Polarimetric sar techniques for remote sensing of the ocean surface *Signal and Image Processing for RS* (CRC Press) pp 284–321
[14] Schuler D, Kasilingam D, Lee J and Pottier E 2003 Studies of ocean wave spectra and surface features using polarimetric sar *Proc. Int. Geosci. and RS Symposium (IGARSS'03)*
[15] Cao F, Hong W, Wu Y and Pottier E 2007 *IEEE Transactions on Geoscience and RS* **45** 3454–3467
[16] Li Y, Xing R, Jiao L, Chen Y, Chai Y, Marturi N and Shang R 2019 *Remote Sensing* **11** 1933
[17] Shah Hosseini R, Entezari I, Homayouni S, Motagh M and Mansouri B 2011 *Canadian Journal of RS* **37** 220–233
[18] Zhang L, Zou B, Zhang J and Zhang Y 2009 *EURASIP Journal on Advances in Signal Processing* **2010** 1–9
[19] Fukuda S and Hirosawa H 2001 Support vector machine classification of land cover: Application to polarimetric sar data *IGARSS 2001. Scanning the Present and Resolving the Future. Proceedings. IEEE 2001 Int. Geoscience and RS Symposium (Cat. No. 01CH37217)* vol 1 (IEEE) pp 187–189
[20] Scikit-learn Svc — scikit-learn 0.24.2 documentation [Online; accessed 22-Jan-2023] URL `https://scikit-learn.org/stable/modules/generated/sklearn.svm.SVC.html`